Observations of Hailstone Characteristics in Multicell and Supercell Thunderstorms

Ian M. Giammanco
Insurance Institute for Business & Home Safety

Tanya M. Brown
Insurance Institute for Business & Home Safety

1. INTRODUCTION

Severe hail events are responsible for nearly $1 billion dollars in annual insured property losses in the United States (Changnon *et al. 2009)*. Despite a general negative trend in population growth across the Great Plains of the United States, an increasing trend in hail-related losses has been observed over the past decade (MunichRe 2013). Despite a decreasing trend in number of hail days per year shown by Changnon *et al.* (2009) the increase in property losses, has generated a renewed interest in understanding how the characteristics of hail may influence damage associated with existing building stock and new construction.

Characteristics of hailstones, such as their size, mass, embryo type, and growth processes have been well documented in the historical literature (Browning 1977; Macklin 1977; Foote and Knight 1977; Knight and Knight 2001). There has been little effort to account for hailstone characteristics other than diameter and mass within engineering applications. It is often assumed that damage states will scale with impact kinetic energy. This is reflected in standardized test methodologies utilizing a steel ball to represent a hailstone (UL 2218). Other test practices use a sphere of clear ice (FM 4473).

It is acknowledged that the degradation of common building materials (e.g. asphalt shingles, vinyl siding, wood shake etc.) with time and environmental exposure likely reduces the ability of a given material to withstand hail impacts.

*Corresponding Author Address: Ian M. Giammanco, PhD. Insurance Institute for Business & Home Safety Research Center, 5335 Richburg Rd, Richburg SC 29729. igiammanco@ibhs.org

Koontz and White (2012) have provided evidence of degraded shingle performance of aged products when subjected to ice sphere impacts. Questions remain regarding the representativeness of laboratory test methodologies to effectively represent the properties of natural hailstones. Differences in observed damage patterns warrant examination of existing methodologies and the exploration of new techniques to adequately represent the characteristics of natural hailstones.

In 2011, the Insurance Institute for Business & Home Safety (IBHS) began a comprehensive research program focused on understanding the damage potential of hail, improving laboratory test methodologies, developing damage functions for a variety of new and aged building components, and evaluating construction practices which may help mitigate losses. A key component to this program has been a field phase in which teams collect in-situ measurements of the characteristics of hail (e.g. primary dimension, secondary dimension, mass, peak compressive force at fracture, photographic catalog; Brown *et al.* 2012). In addition to improving engineering approaches to hail impact testing, the program seeks to understand if the synoptic and mesoscale environments as well as convective mode play a role in the type of hailstone which may be produced (e.g. soft, hard, slushy). The environmental conditions conducive for hail production are well documented (List 1985; Rogers and Yau 1989; Thompson *et al.* 2012);. Examining conditions which yield a harder type of hailstone may help asses which conditions lead to a more damaging hail event.

The 2012 and 2013 field phases have yielded a dataset of 921 hailstones from 22 parent thunderstorms. Figure 1 provides a map of all data collection locations during the 2012 and 2013 field phases.

2. DATA AND MEASUREMENTS

The primary objective of the field teams was to collect and measure representative distributions of hailstones from multiple locations across the swath of hailfall from targeted thunderstorms. The Great Plains region of the United States was selected as the project domain because this area offered good visibility and gridded road networks allowing for safe intercepts of severe thunderstorms. In addition, this region generally experiences more severe hail events than other parts of the U.S (Changnon *et al.,* 2009). Forecast preference was given to regions with the necessary conditions for supercell thunderstorms since this type of thunderstorm exhibits the highest probability for significant hail (Browning 1963; Browning 1977; Lemon and Doswell 1979; Doswell and Burgess 1993). Target storms were selected based on their radar presentation and the ambient environment in which they were embedded. Data were stratified by the general shape of each hailstone and parent thunderstorms were segregated by convective mode according to the decision tree presented by Smith *et al.* (2012).

2.1 *Photographic Catalog, Dimensions, and Mass*

In an effort to collect a robust hail dataset, each hailstone was photographically cataloged in the field based on its collection location and by its associated parent thunderstorm. The dimensions of each stone were measured assuming that two dimensions of the stone ($x_1 \approx x_2$) are relatively similar and larger than the third axis (y). Measuring these dimensions also allowed for a reasonable estimate of the cross-sectional area of the hailstone. Figure 2 provides a diagram of the measured dimensions along with a sample photograph of a measured hailstone. Each stone was also weighed in the field using a digital scale. The photograph of each stone coupled with its physical measurements allowed its shape to be effectively classified. Data were input and stored using a National Instruments LabVIEW user interface which also accommodates measurement equipment and provides a data acquisition interface to measure the compressive force applied to hailstones (Brown *et al*., 2012).

2.2 *Hardness Property*

Throughout historical literature hailstones are often qualitatively referred to as: "hard", "soft" or "slushy" with no quantitative means of describing the hardness of a given stone (Bilhelm and Relf, 1937; Carte 1966; Knight and Knight 1973). It is hypothesized that the hardness property of hail plays a secondary but non-trivial role in damage upon impact. Brown *et al.* (2012) developed a unique piece of instrumentation and test methodology to attempt to fill this observational gap. The 2012 and 2013 field campaigns provided the first opportunity to collect data on the hardness of natural hailstones.

The hardness test measures the applied force on a hailstone until the stone fractures or compresses. The rate of force applied to the stone through the field device is large enough to produce a fast deformation rate and subsequently a brittle failure of the stone. At slow rates of deformation, ice typically exhibits a more ductile failure (Schulson 1997). The measured compressive force at the point of initial fracture is used to calculate the compressive stress values present in this study.

3. OBSERVED HAILSTONE CHARACTERISTICS

3.1 *General characteristics*

The 2012-2013 dataset contains 921 hailstones measured during 14 operation days. The sizes of hailstones measured ranged from as small as 0.25 cm to as large as 10.7 cm. Table 1 provides a summary of each sampled thunderstorm and the associated hail distribution. The cataloged photographs of each stone allowed for a subjective characterization by shape. Each photograph was subjectively reviewed and placed into one of four individual classes: spheroidal, disk, conical, and unclassified. For a hailstone to be classified as a disk its dominant dimension (x_1) was greater than twice that of the measured secondary dimension (y). Spheroidal stones made up 63% of the dataset while 26% were disk-shaped, and conical and un-classified shapes comprised 11% of the dataset (Figure 3). Unclassified stones were often those with large protuberances such that an effective oblateness could not be determined. Spheroidal and disk-shaped stones represent the larger sizes of stones (> 2 cm). All observed conical stones were below 2 cm in diameter, which was in good agreement with Knight and Knight (2001). Every sampled event contained disk and spheroidal stones. All but three cases contained at least one measured conical-shaped stone.

The mean mass of the measured hailstones was 5.8 g with 90% of the dataset falling below 20 g. The most massive stone measured was 163.3 g which was associated with the largest diameter measured. This stone had a diameter of over 10 cm and was found near Ratliff City, OK on 30 May 2013. The relationship between diameter and mass was examined with respect to the four shape classifications. A power-law fit was effective in describing the relationship as shown in Figure 4. The fitted curves accounted for at least 80% of the variance for spheroidal, conical, and unclassified, while the fitted curve for disk-shaped stones accounted for 67% of the variance. The fitted curves provide a means to estimate kinetic energy through basic information such as the diameter of the stone which is often all that is reported following a hail event. These curves should also be applied in risk modeling applications to more effectively represent the potential for building damage within a hail swath. Although not shown, the complete dataset was in good agreement with the historical work of Dennis *et al.* (1971) which also used an exponential curve to describe the mass-diameter relationship.

The compressive stress was used to represent a measure of the hardness of hailstones. Compressive stress values ranged from 9.0×10^{-3} mPa to a maximum of 7.5 mPa. The mean value of the compressive stress distribution was 0.68 mPa with nearly 75% of the dataset falling below 1.0 mPA. All but four cases produced a stone which exceeded 1.0 mPa in compressive stress. The probability distribution is shown in Figure 5. For individual measurement locations within the swath of hailfall for an individual case, the largest compressive stress values were typically not associated with the largest diameter hailstones. The overall range compared well with that found by Haynes (1978) who found a mean compressive strength of ice structures of 1.43 mPa at temperatures of -10 to -20 C. The laboratory results of Field *et al.* (2010) who examined the compressive stress of ice cylinders were also similar. When examined by shape classification, there was no statistically significant difference between the compressive stress distributions for spheroidal, disk, and conical shapes while the unclassified category had a lower mean compressive stress. It is noted though that this class represents the smallest sample size. The use of cross-sectional area may lead to small errors as more irregularly shaped stones may not fracture roughly along this plane. Approximately 9% of the cataloged stones were too spongy or exhibited a ductile failure such that a peak compressive force could not be effectively determined.

3.2 *Convective Mode Influences*

It is well understood that convective mode is a significant contributor to the likelihood and dominant type of severe weather (e.g. tornadoes, large hail, damaging winds). Jewell and Brimelow (2009) has also provided evidence that accounting for updraft longevity and residence times provides an improved forecast of maximum hail size (Knight *et al.* 1982). Given the relatively long time period required for hail growth, updraft longevity plays a role in hail production and its characteristics. A variety of factors contribute to the longevity of thunderstorm updrafts, including proximity to other convection (Jewell and Brimelow 2009; Thompson *et al.* 2012). It is hypothesized that these factors may also govern the hardness of hailstones. The convective modes included in the dataset were examined to determine if any differences in hailstone characteristics might be correlated with convective mode.

The radar-based classification scheme presented by Smith *et al.* (2012) was employed using the Level II WSR-88D archive of radar data for each event sampled. The radar volume immediately prior to the time the target thunderstorm crossed the data collection roadway was used for the classification. The method separates convection into 3 major classes: quasi-linear convective system (QLCS), supercell, and disorganized. Sub-categories are defined within each as shown in Figure 6. A reflectivity threshold of 35 dBZ was used in accordance with Smith *et al.* (2012). Discrete cells were identified by discrete reflectivity values above the threshold with a single dominant updraft. QLCS events were determined as a result of continuous reflectivity at or above the 35 dBZ threshold for at least 100 km, with a length to width aspect ratio of 3 to 1. Disorganized clusters were those which met the reflectivity criteria but did not meet the remaining criteria for either cell type. Additional scrutiny was applied for sub-classifications according to Smith *et al.* (2012).

The characteristics for each major convective mode, excluding the sub-categories, were examined and are provided in Table 2. The typical convective mode sampled during the 2012-2013 field phase was supercells. Given the target preference toward environments supporting supercells the dataset is biased towards this storm mode (746 hailstones from identified supercells). Additional effort is needed to adequately sample linear storm modes. However, linear storm modes present significant data collection and logistical challenges compared to more discrete storm structures.

As expected, supercell events produced the largest hail sizes; however, their mean compressive stress value was 0.76 mPa, less than that found for the disorganized cell classification which had a mean value of 1.53 mPa. It is noted that the sample size for the disorganized classification is 33 hailstones from only two parent thunderstorms. The mean compressive stress of the QLCS group was 0.46 mPa for 142 hailstones from four separate events. The hail shape distributions for supercell and QLCS events did not significantly deviate from the overall dataset. The dominant shape for both storm types was spheroidal (~ 60%).

Given the large supercell sample size, the sub-classifications according to Smith *et al.* (2012) were applied. Table 3 provides the summary statistics for each supercell sub-classification. A "supercell in a cluster – right mover" was the most common sub-classification with over 68% of the hailstones measured from events falling in this category. The single left moving discrete supercell case produced the largest mean compressive stress of 1.6 mPa with nearly all measured stones falling into the spheroid shape classification (23 of 30 stones). The discrete right moving supercell cases (4) exhibited the lowest mean compressive stress value (0.39 mPa) which also fell below that for the QLCS group. Interestingly, the right mover discrete and marginal discrete sub-classifications had the smallest standard deviations (Figure 7). For right moving supercells, the compressive stress values were typically clustered by parent updraft with small standard deviations in compressive stress for the distribution of measured stones. The sample size remains too small to make any significant conclusions and it is unclear if the measurements collected by the field teams are truly representative of a random sample of the hail distribution.

4. LABORATORY COMPARISONS

The use of ice spheres to represent hailstones in standardized test methodology (FM 4473 warranted a comparison with field observations. Ice spheres were made using spherical molds of 3.175 cm (1.25 in.), 4.445 cm (1.75 in), and 5.715 cm (2.25 in.). While the FM 4473 test standard requires distilled water, both tap and distilled water were used. The molds were placed in a freezer at approximately -20° C for 24 hours. Laboratory stones were measured and weighed in the same fashion as was conducted in the field. A laboratory version of the field device was developed and used for the compressive force test. This device features the same instrumentation components as the field version with an approximate measurement error of ±0.4 N in applied force.

The mass-diameter relationship was examined for the laboratory ice spheres and the field dataset. The results are shown in Figure 8. The tap and distilled water stones were biased towards a higher mass given a similar diameter, as compared to the field hailstones. The primary cause is the use of purely spherical laboratory stones versus the shape distribution of the measured hailstones previously discussed. The 37% of field data which were not spheroidal contributed to the difference. Laboratory ice spheres also were predominately clear ice with small trapped bubbles and very small expansion cracks. The photographs of the natural hail revealed a larger percentage of trapped bubbles as well as the classic layered structure as a result of alternating growth processes (Knight and Knight 2001). Additional solutions using dissolved CO_2 to produce a larger percentage of trapped bubbles were used with little statistical difference in results. Spheres comprised of compacted crushed ice were also investigated, and generally resulted in harder laboratory ice spheres. These experiments are summarized in Giammanco and Brown (2013). The presence of expansion cracks in laboratory spheres led to variability in the compressive stress measurements as stones often crack along pre-existing fractures.

Although a noted difference was observed in the mass-diameter relationship, when the compressive stress was examined, laboratory ice spheres fell very close to the mean of that observed in the field. Field data were binned by equivalent diameter using 0.635 cm (0.25 in.) bin sizes for comparison with the three sizes of laboratory ice spheres. Compressive stresses were plotted for binned groups of the individual laboratory datasets and the field dataset, shown in Figure 9. It is readily apparent that the mean compressive stresses of the field data are similar to tap and distilled water ice spheres produced in a laboratory setting. These stones represent a reasonable approximation of the mean compressive stress of natural hailstones observed in the Great Plains region during the 2012-2013 campaign. Despite a general clustering of compressive stress values for discrete storm modes, most cases in which additional convection was in close proximity exhibited large variability.

5. SUMMARY

The data collected during the 2012 and 2013 IBHS field phases has provided a much needed baseline to evaluate the representativeness of existing laboratory test methodologies. The compressive force test applied to natural hailstones has also provided a quantitative means to describe the hardness property of a given stone. The overall sample size from the two years of field measurement is miniscule compared to the number of stones a single thunderstorm can produce.

Spheroidal shapes were the dominant type of hailstone encountered with a quarter of the dataset being disk-shaped. These two predominant shapes were observed in all parent thunderstorms. The typical size of stone measured during the two year field phase was approximately 2 cm with 60% of the dataset falling below the National Weather Service's severe threshold (2.54 cm / 1 in). Mean compressive stresses measured in the field were generally similar to those found in laboratory testing of clear ice but exhibited a large range. The stratification of data by convective mode yielded some interesting preliminary results. Discrete cells typically produced the largest maximum size stones but typically lower compressive stress values and a smaller range. Cells within a cluster produced the largest compressive stress values. For non-supercell modes the sample size was far too small to apply any sub-classifications. A significant amount of data is needed for both supercell and non-supercell convective modes to effectively evaluate any statistical differences.

The comparison between laboratory and natural hailstones yielded interesting results. The relationship between mass and diameter suggests that the kinetic energy of laboratory stones is higher than stones of a similar diameter observed in the field. This is a result of the varying shapes observed in the field and their associated mass-diameter curves versus pure ice spheres used in laboratory testing. For impact tests, the use of propulsion speeds derived from terminal velocity estimates of natural hailstones or assuming a perfect sphere would yield a higher kinetic energy than a natural stone falling at the same velocity. It is intuitive that larger, more massive stones will produce more damage through increased kinetic energy. It is also understood that the steel ball laboratory method for hail impacts (UL 2218) produces damage patterns which are different than those observed in the field. The contribution of the hardness property of hailstones and how it relates to the imparted force and duration of impact is not well understood. Future work will continue to focus on understanding this contribution and how common building materials perform in their new and aged states.

REFERENCES

Bilhelm, E.G., and E.F. Relf, 1937: The dynamics of large hailstones. *Quart. J. Roy. Meteor. Soc.,* **63**, 149-162.Brimelow, J.C., T.W. Krauss, and G.W. Reuter, 2002: Operational foreca*sts of maximum hailstone diam***et**er in Mendoza, Argentina. *J. Wea. Mod.*, **34**, 8-17.

Brown, T.M., I.M. Giammanco,and D.S. Robinett, 2012: Observations of hailstone characteristics utilizing a new instrumentation platform. *26th Conference on Severe Local Storms,* Nashville, TN.

Browning, K.A., 1963: The growth of large hail within a steady updraught. *Quart. J. Roy. Meteor. Soc.*, **89**, 490-506.

Browning, K.A., 1977: The structure and mechanisms of hailstorms: *A review of hail science and suppression, Meteor. Monogr.*, No. 38, Amer. Meteor. Soc., 1-43.

Browning, K.A. and G.B. Foote, 1976: Airflow and hail growth in supercell storms and some implications for hail suppression. *Quart. J. Roy. Meteor. Soc.*, **102**, 499-533.

Carte, A.E., 1966: Features of Transvaal hailstones. *Quart. J. Roy. Meteor. Soc.,* **92**, 290-296.

Changnon, S.A., D. Changnon, and S.D. Hilberg, 2009: Hailstorms across the nation: An atlas about hail and its damages. Illinois State Water Survey Contract Report 2009-12, 78 pp.

Dennis, A.S., P.L. Smith Jr., G.A.P. Peterson, and R.D. McNeil, 1971: Hailstone size distributions and equivalent radar reflectivity factors computed from hailstone momentum records. *J. Appl. Meteor.,* **10,** 79–85.Doswell III,

C.A. and D.W. Burgess, 1993: Tornadoes and tornadic storms: A review of conceptual models. *The Tornado: Its Structure, Dynamics, Prediction, and Hazards, Geophys. Monogr.*, No. 79, Amer. Geophys. Union, 161-172.
Edwards, R. and R.L. Thompson, 1998: Nationwide comparisons of hail size with WSR-88D vertically integrated liquid water and derived thermodynamic sounding data. *Wea. Forecasting*, **13**, 277-285.

Field, P.R., W. Hand, G. Cappelluti, A. McMillan, A. Foreman, D. Stubbs, and M. Willows, 2010: *Hail threat standardization.* European Aviation Safety Agency, Technical Report EASA.2008/5. 130 pp.

FM Approvals. (2005). Specification test standard for impact resistance testing of rigid roofing materials by impacting with freezer ice balls (FM 4473). West Glocester, RI: FM Approvals.

Foote, G.B., 1984: A study of hail growth utilizing observed storm conditions. *J. Climate. Applied Meteor.*, **23**, 84-101.

Foote, G.B., and C.A. Knight Eds., 1977: *Hail: A Review of Hail Science and Suppression.* Meteor. Monogr. No. 38, Amer. Meteor. Soc., 277 pp.

Giammanco, I.M., and T.M. Brown, 2013: *Characteristics of Severe Hail 2012 Pilot Field Study: Data Analysis Summary* (IBHS-RC03-2013). Tampa, FL: IBHS.

Haynes, F.D., 1978: Effect of temperature on the strength of snow-ice. Department of the Army, Cold Regions Research and Engineering Laboratory, Corps of Engineers, CRREL Report 78-27: Hanover, New Hampshire.

Jewell, R., and J.C. Brimelow, 2009: Evaluation of Alberta hail growth model using severe hail proximity soundings from the United States. *Wea. Forecasting*, **24**, 1592–1609.

Knight, C. A., W. A. Cooper, D. W. Breed, I. R. Paluch, P. L. Smith, and G. Vali, 1982: Microphysics. *Hailstorms of the Central High Plains,* C. Knight and P. Squires, Eds., Vol. 1, Colorado Associated University Press, 151–193.

Knight, C.A., and N.C. Knight, 1973: Quenched, spongy hail. *J. Atmos. Sci.,* **30**, 1665-1671.

Knight C.A. and N.C. Knight, 2001: Hailstorms in severe convective storms Ed. Doswell C.A., *Amer. Meteor. Soc.*, Monograph, 223-254.
Koontz, J.D. and T.L. White, 2012: The correlation between hail resistances and the physical properties of fiberglass shingles. *International Roofing Exposition,* San Antonio, TX, 16 pp.

Lakshmanan, V.,T. Smith, G. Stumpf, K. Hondl, 2007: The Warning Decision Support System - Integrated Information. *Wea. Forecasting*, **22**, 596-612.

List, R., 1985: Properties and growth of hailstones. *Thunderstorm morphology and dynamics*, E. Kessler Ed., University of Oklahoma Press, 259-276.

Lemon, L.R., and C.A. Doswell III, 1979: Severe thunderstorm evolution and mesocyclone structure as related to tornadogenesis. *Mon. Wea. Rev.*, **107**, 1184-1197.

Macklin, W.C., 1977: The characteristics of natural hailstones and their suppression. *Hail: A Review of Hail Science and Suppression, Meteor. Monogr.*, No. 38, Amer. Meteor. Soc., 65-88.

Rogers, R.R., and M.K. Yau, 1989: *A Short Course in Cloud Physics.* 3d ed Elsevier, 290 pp.

Schulson, E.M., 1997: The brittle failure of ice under compression. *J. Phys. Chem. B*, **101**, 6254-6258.

Thompson, R.L., B.T. Smith, J.S. Grams, A.R. Dean, and C. Broyles, 2012: Convective modes for significant severe thunderstorms in the contiguous United States. Part II: Supercell and QLCS tornado environments. *Wea. Forecasting*, **27**, 1136 -1154.

Smith, B.T., R.L. Thompson, J.S. Grams, and C. Broyles, 2012: Convective modes for significant severe thunderstorms in the contiguous United States. Part I: Storm classification and climatology. *Wea. Forecasting*, **27**, 1114-1135.

Underwriters Laboratory, 2012: *UL 2218: Standard for impact resistance of prepared roof covering materials.* Northbrook, IL: UL.

Witt, A., M.D. Eilts, G.J. Stumpf, J.T. Johnson, E.D. Mitchell, and K.W. Thomas, 1998: An enhanced hail detection algorithm for the WSR-88D. *Wea. Forecasting*, **13**, 286–303.

Table 1. Summary statistics for each thunderstorm event during the 2012-2013 field phase.

Case	Date	Location	Sample Size	Max Diameter (cm)	Mean Diameter (cm)	Max Compressive Stress (mPa)	Mean Compressive Stress (mPa)
1A-2012	5-27-12	Ravenna, NE	5	1.93	1.35	1.33	0.88
2A-2012	5-28-12	Lindsay, OK	32	4.75	2.77	2.21	0.89
3A-2012	5-29-12	Kingfisher, OK	20	7.75	2.31	3.71	1.24
3B-2012	5-29-12	Greenfield, OK	17	3.05	1.93	4.32	1.31
4A-2012	6-1-12	Channing, TX	45	3.12	1.80	4.20	0.85
5A-2012	6-2-12	Eads, CO	17	3.33	1.63	0.76	0.39
*6A-2012	6-6-12	Cheyenne, WY	36	3.23	1.44	0.54	0.22
7A-2012	6-7-12	LaGrange, WY	8	3.76	3.12	0.64	0.38
*7B-2012	6-7-12	LaGrange, WY	59	5.41	3.02	2.77	0.57
*1A-2013	5-17-13	Hyannis, NE	85	3.30	1.41	4.57	0.81
2A-2013	5-18-13	Paradise, KS	6	1.82	0.96	0.41	0.40
*3A-2013	5-19-13	Wichita, KS	112	3.20	1.47	4.24	0.61
3B-2013	5-19-13	Arkansas City, KS	16	3.43	1.51	1.51	0.64
*3C-2013	5-19-13	Blackwell/Newkirk, OK	23	2.51	1.11	1.51	0.55
*3D-2013	5-19-13	Cedar Vale, OK	71	3.99	2.08	1.12	0.29
3E-2013	5-19-13	Burbank, OK	18	2.21	1.11	1.80	0.95
*4A-2013	5-20-13	Antioch, OK	212	4.80	0.81	3.34	0.56
5A-2013	5-30-13	Blanchard, OK	15	3.98	2.08	1.58	0.59
*5B-2013	5-30-13	Ratliff City, OK	29	10.69	2.61	3.88	0.70
6A-2013	6-1-13	Mason, TX	29	2.99	1.60	7.46	1.64
6B-2013	6-1-13	London, TX	30	3.60	1.88	6.46	1.43
7A-2013	6-2-13	Elmwood, OK	36	3.71	1.88	2.86	0.51

**multiple measurement locations within the swath of hailfall from the same parent updraft*

Table 2. Summary statistics for each primary convective mode classification.

Convective Mode	Events	Sample Size	Max Diameter (cm)	Mean Diameter (cm)	Max Compressive Stress (mPa)	Mean Compressive Stress (mPa)
QLCS	4	142	3.99	2.27	2.90	0.46
Supercell	19	746	10.69	2.41	6.46	0.76
Disorganized	2	33	3.12	1.87	7.46	1.53

Table 3. Summary statistics for supercell sub-classifications.

Sub-classification	Events	Sample Size	Max Diameter (cm)	Mean Diameter (cm)	Max Compressive Stress (mPa)	Mean Compressive Stress (mPa)
Discrete – RM	3	59	10.7	2.58	0.99	0.31
Discrete – LM	1	30	4.74	3.24	5.64	1.60
Cell in cluster - RM	7	514	7.75	2.37	7.57	0.79
Cell in cluster - LM	0	N/A	N/A	N/A	N/A	N/A
Cell in line - RM	0	N/A	N/A	N/A	N/A	N/A
Cell in line - LM	0	N/A	N/A	N/A	N/A	N/A
Marginal discrete	2	36	3.60	2.32	1.15	0.68
Marginal cell in cluster	4	107	3.77	2.13	6.18	0.66
Marginal cell in line	0	N/A	N/A	N/A	N/A	N/A

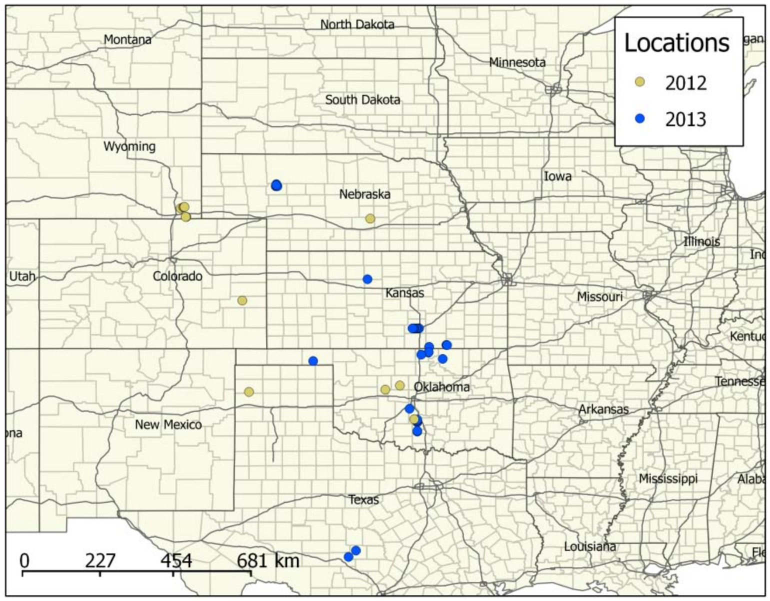

Figure 1. Map of all measurement locations during the 2012 (yellow) and 2013 (blue) field phases.

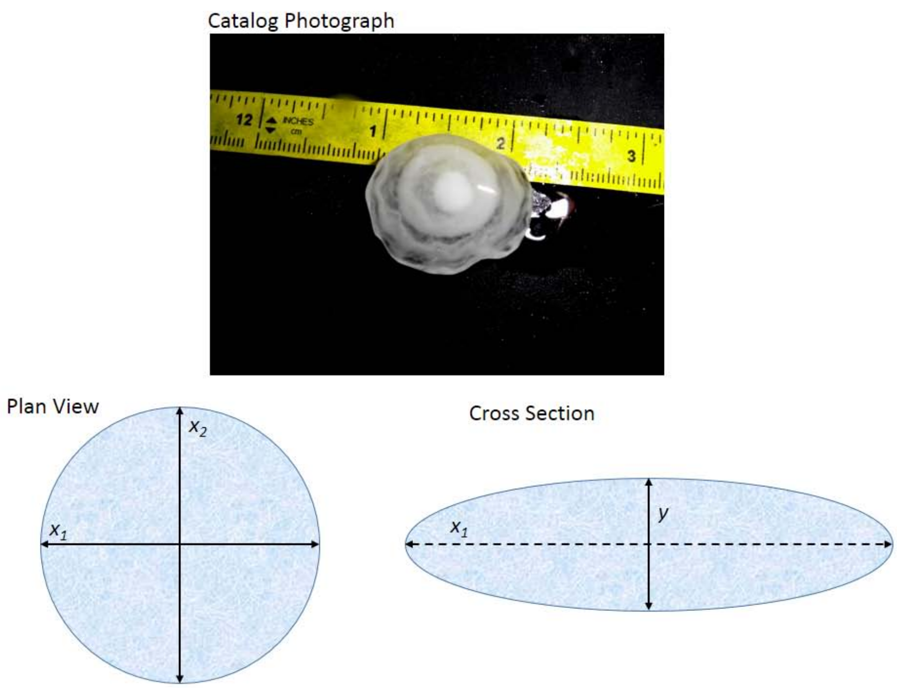

Figure 2. Example of a hail stone catalog photograph (top) and diagram of measured hailstone dimensions (bottom).

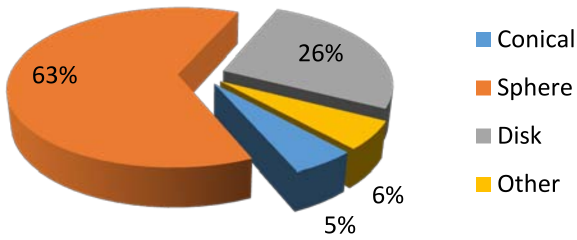

Figure 3. Observed hailstone shape classifications during the 2012-2013 field phases.

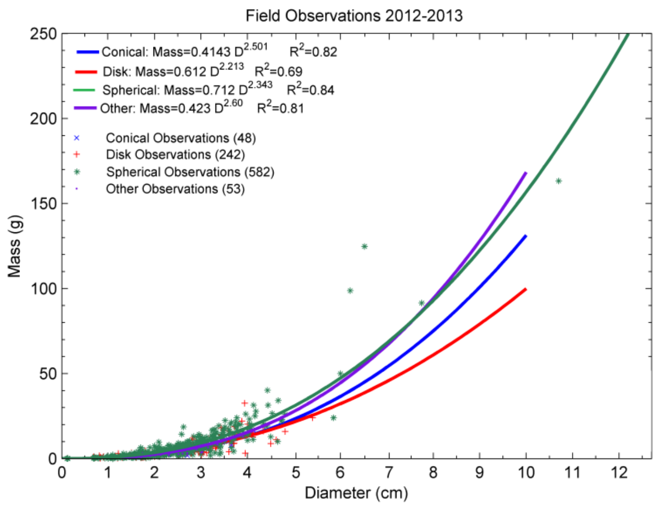

Figure 4. Mass shown as a function of diameter for 2012-2013 field observations stratified by shape classification. Exponential fits (solid) for each shape class are also shown.

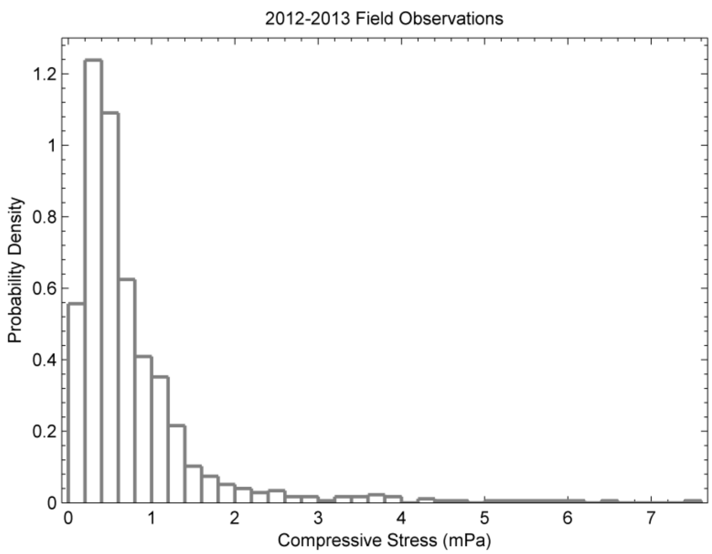

Figure 5. Hailstone compressive stress distribution for 2012-2013 field observations.

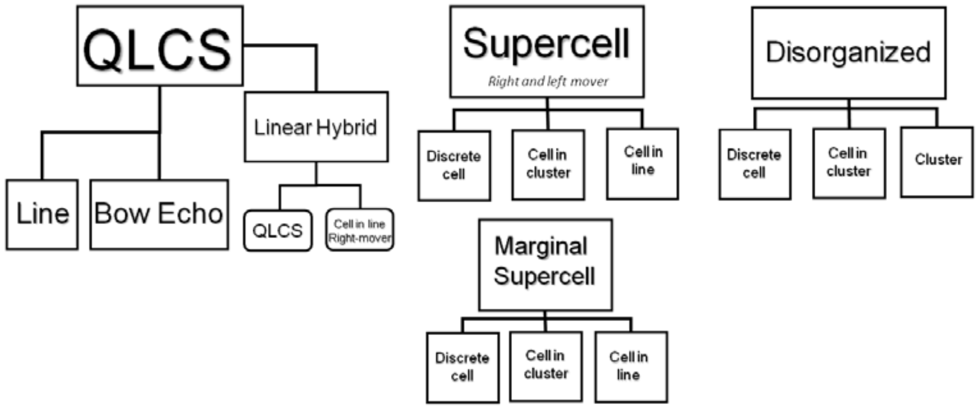

Figure 6. Primary and sub-classifications for the convective mode decision tree described by Smith *et al.* (2012).

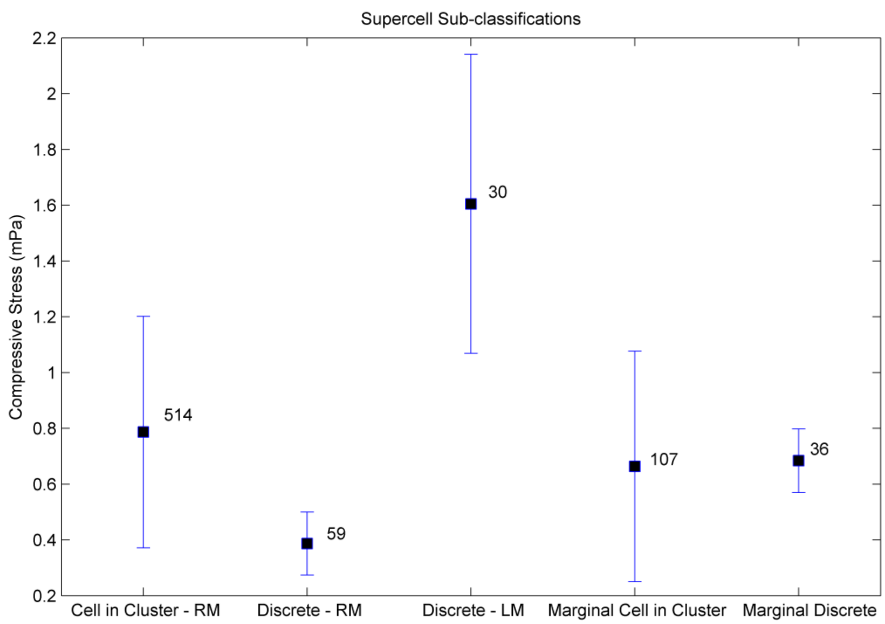

Figure 7. Mean compressive stress for each supercell sub-classification. Error bars represent ± 1 standard deviation from the mean. The sample size for each sub-classification is also provided.

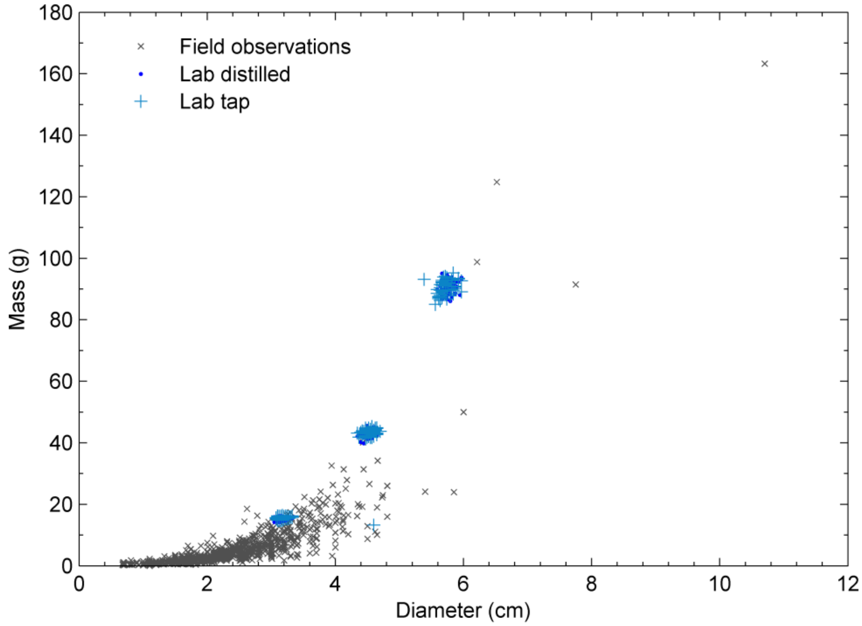

Figure 8. Measured mass shown as a function of diameter for 2012-2013 field observations (gray), laboratory tap water ice spheres (dark blue), and laboratory distilled water ice spheres (light blue).

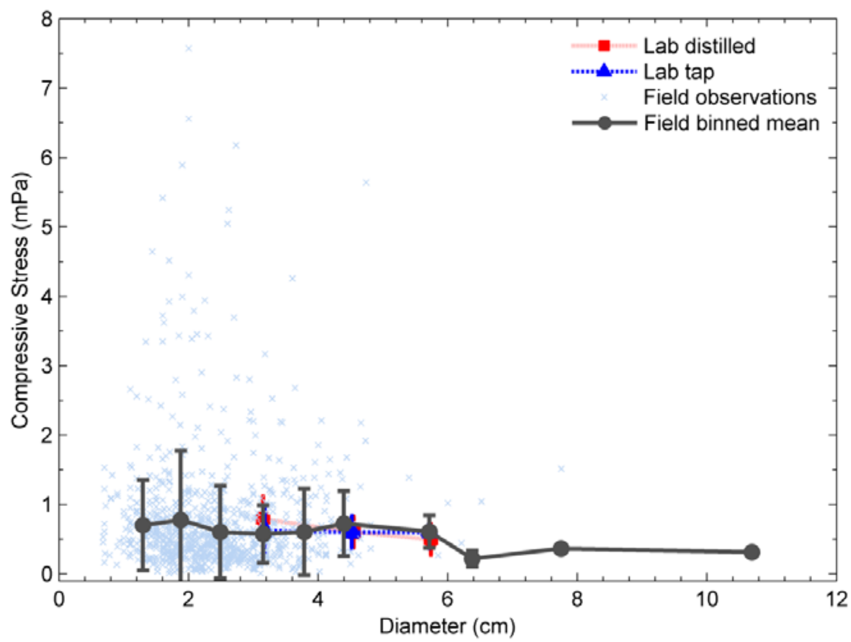

Figure 9. Compressive stress shown as a function of diameter for 2012-2013 field observations (light blue), field observations binned by diameter (solid gray), laboratory tap water ice spheres (blue), and laboratory distilled water ice spheres (red). Error bars represent ±1 standard deviation from the mean for each group.